IPNS Neutron Scattering Instrument Development

C.S. Borso, R. Brenner, T.O. Brun, J.M. Carpenter, R.K. Crawford, J.E. Epperson, G.P. Felcher, D.G. Hinks, G. Holmblad, J.D. Jorgensen, R. Kleb, G.A. Lander, M.H. Mueller, G.E. Ostrowski, C.A. Pelizzari, F.J. Rotella, A.J. Schultz, M.G. Strauss, R.G. Teller, F. Williamson, T.G. Worlton.

Argonne National Laboratory
9700 South Cass Avenue
Argonne, Illinois 60439

The ZING-P' Prototype has been used for the development of five types of instrument: (a) crystal analyzer spectrometer (b) chopper spectrometer (c) single crystal diffractometer (d) small-angle diffractometer and (e) high-resolution powder diffractometer. These five types comprise the initial group of seven IPNS-I instruments, the chopper spectrometers existing in high-resolution and high-intensity forms and the powder diffractometers in special-environment and general-purpose forms. In addition, we have also worked on (f) the development of resonance-neutron radiography (which, although not a scattering instrument, is convenient to discuss here), (g) area neutron-position detectors, and (h) polarized neutron instrumentation, as well as (i) the data acquisition system for IPNS-I. We will briefly summarize some of these developments.

A. Crystal Analyzer Spectrometer

The crystal analyzer spectrometer at ZING-P' was very active during the last operating cycle, partly because of the high neutron flux available during that period. Approximately 75% of the available beam time was spent on problems generated by outside users. The experiments performed include studies of:

1. Phonondensity of states of HCOOH at 25 K and 235 K with C. V. Berney and S. H. Chen (M.I.T.).
2. Phonon density of the water of hydration in RNA with G. Ascarelli, and G. Nucifora (Purdue).

3. Phonons in pyrolytic graphite with W. Kamitakahara (Iowa State Univ.).
4. Hydrogen vibrations in $LaH_x(D_x)$ and $CeH_x(D_x)$ with W. Kamitakahara (Iowa State Univ.).
5. Hydrogen vibrations in $VH_{0.75}$ with K. Ross (Univ. of Birmingham, England).
6. Tunneling modes in CsH_2PO_4 with R. Youngblood (Brookhaven National Laboratory).
7. Vibrational frequency spectrum of H in VH_x as a function of temperature. Fig. 1 shows a spectrum obtained with $VH_{0.02}$ at 30 K.

B. Chopper Spectrometer

Inelastic scattering spectra were taken at the Chopper Spectrometer for a sample of UN at room temperature using two incident energies, E_o = 130 meV and 307 meV. The new Fermi chopper designed by Robert Kleb was used in both cases. This chopper, which will be used in Low-Resolution Medium-Energy Chopper Spectrometer (LRMECS) at IPNS-I, performed as predicted at these neutron energies and is expected to prove satisfactory for neutrons of energy 1 eV or higher. One of the spectra is shown in Fig. 2. The large-Q spectra (taken at a scattering angle of 85°) show well-defined peaks from the nitrogen vibration mode, including at least the second harmonic at 90 meV in the E_o = 307 meV run. At small Q (7.5° scattering angle) the nigrogen mode is much weaker, as expected.

Information obtained in the operation of the Chopper Spectrometer is now being used to optimize the design of choppers and shielding for the IPNS-I chopper spectrometers.

C. Single Crystal Diffractometer

For the last 6 weeks of ZING-P', data were measured continuously on the time-of-flight single crystal diffractometer. Nearly 50 histograms were obtained

on a disk-shaped NaCl crystal (3 mm high x 4 mm diameter). These data cover a complete hemisphere in reciprocal space and will be used for developing software for converting raw integrated intensities into structure factors. Although the data were collected with a 20 x 20 cm position sensitive ^3He gas-filled detector, Figs. 3 and 4 are typical histograms and peak profiles. Other data were also collected on a crystal of $LiNH_4SO_4$.

One of our major efforts in the past few months has been the development of software which will permit fast and efficient data collection. A flow diagram for data collection is shown in Fig. 5. A crystal with an unknown unit cell is mounted on the difframtometer in an arbitrary orientation. Counts are accumulated for a histogram, which is then searched for Bragg peaks. The interpolated positions of the Bragg peaks are used in an auto-indexing program written by R. Jacobson (Iowa State University) which provides an orientation matrix and cell parameters. The positions of any number of Bragg reflections can be used in a least-squares procedure to obtain highly accurate cell parameters.

A table of diffractometer χ and ϕ setting angles are calculated using a program written by H. Levy (Oak Ridge National Laboratory). The settings provide coverage of a hemisphere of reciprocal space with minimum overlap. Each histogram is counted for a preset monitor count at which point the crystal is reoriented by driving χ and ϕ and a new histogram is started. Integrated intensities are obtained by calculating the location of reflections in each histogram and integrating in three dimensions. These data are then reduced and normalized to obtain structure factors for the structure solution and refinement.

D. Small Angle Diffractometer

The Small Angle Diffractometer at ZING-P' incroporated a multiple-converging-aperture collimator constructed of tapered stainless steel tubes. Gd_2O_3-epoxy

paint on the inside and outside prevented internal reflections and "cross talk" between tubes which were enclosed in a 10 cm diameter pipe filled with boric acid solution. The same detector and data acquisition system were used as for the Single Crystal Diffractometer. The diffractometer was used for two test measure ments, on cetylpyridinium chloride (described below) and on an irradiated single crystal of aluminum.

Cetylpyridinium chloride is a lipophilic compound which is known to form micellar structures in a variety of polar solvents. It thus serves as an excellent model system for the study of the aggregation and transport properties of these structures. The molecular structure

consists of a long hydrocarbon chain connected to a polar head group consisting of an aromatic ring.

The electron density of these structures is closely matched to that of water and thus X-ray studies have been difficult to perform. Several similar molecules have been studied with X-ray small angle scattering using various solutes to enhance the contrast of the molecule. Using these same X-ray techniques with CPC yields a classical small angle scattering curve characteristic of micelles. Using neutron scattering in 100% D_2O, however, as shown by our results at ZING-P' (Fig. 6), quite a different structure occurs at the same CPC concentration. We are continuing this study with further neutron experiments at University of Missouri and with SAXS and NMR at Argonne to fully characterize the structural properties of CPC.

E. High Resolution Powder Diffractometer

We first began collecting data on the High Resolution Powder Diffractometer (HRPD) at ZING-P' in July 1978. From that time until the final shutdown of ZING-P' in August 1980, 104 sets of time-of-flight diffraction data were collected on the HRPD, which represents work on 54 separate samples. Of the 54 experiments performed, 37% were proposed by collaborators from outside of Argonne, 15% were experiments on standard samples for instrumental characterization and calibration, and the remaining 50% were suggested by scientists here at Argonne.

The types of experiments performed on the HRPD were scientifically quite diverse. The utility of powder techniques as a structural tool was investigated by comparison of powder and single crystal neutron diffraction results on well-characterized samples. A study of the effect of the temperature on solid state structure, especially atomic thermal motion, was undertaken by comparing diffraction results on samples at room temperature and near the temperature of liquid helium. Samples which exhibit phase transitions induced at either above (to 1000°K) or below (to 10°K) room temperature were studied. Structural studies were carried out on electrical conductors -- ternary superconductors, fast-ion conductors and one-dimensional conductors and battery materials (see Fig. 7). Powder data were taken on samples of metal deuteride compounds in order to locate deuterium positions in the structure via Fourier synthesis. The structure of substances which are known to be active in the catalysis of certain types of chemical reactions were investigated.

Work done on the HRPD over the last two years has given a much better indication of the limits of the time-of-flight neutron powder techniques and the analysis of data therefrom, which will be invaluable in the design and operation of the powder diffractometers at IPNS-I. The ability to collect data on samples

in special environments -- at temperatures to 10° K in a closed-cycle DISPLEX refrigerator, at temperatures in excess of 900° K in a specially designed furnace and with a powder sample in an in situ liquid electrochemical cell -- was demonstrated. Strains as low as 0.2% were measured on the HRPD, and the extremely high-resolution of the HRPD also made evident inhomogeneities and impurities in some samples seen as homogeneous by other analytical tools. HRPD powder data have been analyzed using a time-of-flight version of the Rietveld profile refinement program, written by R. B. vonDreele at Arizona State University and modified and augmented here at Argonne. To date, 48% of all data taken on the HRPD have been analyzed, with many of our collaborators taking an active role in the actual analyses. This time-of-flight Rietveld code will be used as a prototype for the future data analysis software package that will be operative at IPNS-I. A standard Fourier synthesis program has been adapted to this Rietveld code, and with it, we have demonstrated the ability to generate maps of the nuclear density distribution in a solid from powder data.

F. Resonance Neutron Radiography

Radiography has been for many years one of the important applications of neutron beams. A pulsed source offers a unique advantage for certain applications of radiography because the various energies can be readily separated by time-of-flight techniques. Many nuclei exhibit neutron resonances in the epithermal region and our aim is to identify these nuclei in a target material by their absorption of neutrons at a specific resonant energy. The basic requirements for such a technique are a source of pulsed epithermal neutrons and a position-sensitive detector capable of high data rates and accumulation of data into x, y and t ($\propto E^{-1/2}$) channels. The NPSD described below is just such a detector.

To demonstrate the method, we describe briefly the test experiment at the ZING-P' facility in July 1980. The target, consisting of foils of Au and In, is shown in Fig. 8. In Fig. 9(a) we show the transmission profile from 1-7.5 eV, i.e., the intensity of neutrons summed over all the detector as a function of time-of-flight from the time t_o when the proton pulse hits the target. Here we identify three resonance energies, two associated with In and one with Au. In Fig. 8 we examine the spatial dependence of these resonances by looking at the response of the detector at a given time channel. In the top view the 5.7 eV neutrons essentially give the beam profile as the target is transparent at this energy, the center and lower views show the In and Au positions, respectively. Note the overlap from channel 125-135 corresponding to the fact that in the center the target is opaque to both 1.46 eV (In) and 4.91 eV (Au) neutrons. Finally, we attempted a very rapid test on two fuel pellets. A transmission profile is shown in Fig. 9(b). This is more complex than Fig. 9(a) but we can readily identify ^{239}Pu, ^{235}U, ^{238}U, and ^{241}Am from the Pu decay.

These tests have proved that the method can work at IPNS-I and efforts are now underway to identify specific applications.

We appreciate the help of J. Reddy and R. L. Hitterman (MSD).

G. New Neutron-position Scintillation Detector

A new, two-dimensional, neutron-position scintillation detector (NPSD) is being developed at Argonne to meet the growing needs of scattering experiments at IPNS-I. The NPSD is based on the well-proven principle of the Anger γ-ray camera and has a number of important advantages over the conventional gas detectors. In particular, because there is no need for high pressure gas, the detector can be made much more efficient in the epithermal regime and, compared to the gas detector, the parallax of the NPSD is appreciably less and the construction is easier and therefore cheaper.

The NPSD was evaluated at ZING-P' in scattering experiments and resonance radiography.

Figure 10 shows on the left a perforated Cd mask with 2.75 mm holes spaced 10 mm apart along the X and Y axes. The mask was attached to the face of the detector which was at 90° with respect to the beam. A vanadium rod was placed in the beam 20 cm away from the detector to produce isotropic scattering. The scattered neutrons incident on the Cd mask produced the image on the right in Fig. 10. The image clearly shows all the holes.

Figure 3 shows a Laue pattern of a NaCl crystal containing all reflections between 0.7-4 A. The detector was at 90° with respect to the beam and 20 cm away from the crystal. The peak in the middle, right of center, is a superposition of four reflections. The second (right) and the third (left) order reflections are shown on the bottom.

Figure 4 shows the X and Y profiles of the Bragg peak in the lower left of Fig. 3. The peak widths reflect the intrinsic resolution of the detector (2-3 mm) and the broadening effects due to the crystal size (3 mm diameter), mosaic structure, and beam collimation and divergence.

The potential of the detector as an imaging device for resonance neutron radiography was evaluated by flooding a 3 mm thick $^{10}BC_4$ test pattern, placed on the face of the detector, with thermalized neutrons from a Pu-Be source located 2.5 m away. A photograph of the test pattern is shown on the left of Fig. 11. Its center section is comprised of 2 mm wide slits on the right and 4 mm wide bars on the left with disks and holes above and below. The image produced by the detector as observed on the CRT, after correction for nonuniformity by the computer, is shown on the right. Note that even with this first detector all the features are clearly visible. The high stability of this detector is reflected

in the good delineation seen in this image which was obtained over an 18 h period. The use of this detector in a resonance radiography experiment is described above.

H. Polarized Neutron Instrumentation

The availability of a "white" beam of polarized neutrons at IPNS would make possible novel experiments, such as the study of high-energy electron excitations in metals. Polarization of the beam can be obtained by passing it through a suitable filter, most typically a target material that contains a high concentration of polarized hydrogen nuclei. We have chosen as target a crystal of yttrium ethyl sulfate doped with ytterbium. Here high proton polarization is attained due to coupling of the proton spins with the magnetic impurity ytterbium (kept polarized by an external magnetic field) by a method called "spin refrigeration". We are presently assembling a prototype spin refrigerator, and in the near future we will test the achieved proton polarization by SQUID magnetometry. Subsequently, the efficiency of the device as a neutron spin filter will be tested in collaboration with C. Olsen at the WNR facility at Los Alamos. The device has the potential of eventually achieving ~75% proton polarization in an easily reachable sample environment (temperature ~1.1 K; applied magnetic field ~14 kG). This may also proved to be an attractive way to filter neutron spins well above the epithermal range of energy used in Solid State research; hence it might be useful for nuclear physics programs.

A study of the best utilization of the polarized beam of neutrons at IPNS has generated the concept of a novel kind of instrument, the "spin precession resonance spectrometer". Its function is the detection of medium and high energy excitations in solids at small momentum transfer. For these processes the energy and momentum conservation laws require not only a high energy E_i for the incident

neutrons but a high energy E_f for the scattered neutrons. The instrument is basically a resonance spectrometer. The detector consists of a target that absorbs neutrons only in an energy window $E_R \pm \Delta E_R$ surrounded by photomulitpliers which detect the ensuing burst of gamma rays. The machine in this simple form provides a resolution of E_f defined by the width of the resonance line, but this is too wide for a large number of experiments. The compression of ΔE_f is achieved in the following way: The initial beam is fully polarized, and the detector contains a target having a spin-dependent resonance. If the target is also fully polarized, it will analyze both the energy and the spin of the scattered neutrons. The compression of ΔE_f is achieved by inserting a short-spin precession unit, similar in form and function to that developed at I.L.L. in the spin-echo spectrometer, along the path of the scattered neutrons. In this way, ΔE_f is controlled by the maximum magnetic field available in the precessing unit. As an added bonus spin-flip processes (such as the scattering from magnetic excitations and nuclear spin incoherent scattering) can be separated from non-spin-flip processes. The first estimates of the luminosity and resolution attainable by this machine are promising. Further research and the acquisition of state of the art technology is required before its realization.

I. Data Acquisition System

Hardware and software procurement and development for the Data Acqusition System (DAS) for IPNS Neutron Beam Instruments is proceeding under the direction of the IPNS DAS Development Team, which includes hardware and software specialists and neutron scattering scientists.

The DAS will be in a "star" configuration as shown in Fig. 12 with a minicomputer and data collection system for each instrument connected to a central "Host" computer through independent data lines. The Host computer will be a

32-bit VAX 11/780 with a Floating Point Accelerator and 0.5 MB of memory. It will have an RM03 67 MB Disk Drive and a TU77 125 ips dual density magnetic tape unit. It will also have hard copy terminals, video terminals, graphics terminals, a Versatec Printer/Plotter and modems for remote communications. The star configuration has the advantage of independent data collection and centralized processing power and allows the more expensive peripherals to be concentrated on one machine. Most Host computer software will be in FORTRAN and will be run under the VAX VMS operating system.

Each Minicomputer System will have a 16 bit DEC PDP 11/34A minicomputer for experiment control and for communication with its Data Collection System and with the Host. The Minicomputer System software will also be mostly in FORTRAN and programs will execute under the RSX11M operating system. Programs and data will be stored on an RL02 10 MB capacity disk. Each Minicomputer System will include an LA120 180 character per second hard-copy terminal and a VS11 graphics terminal. A typical Minicomputer System is shown in Fig. 13.

Each Data Collection System will include a CAMAC System containing a Time-Digitizer Module, a Master Clock Module, Polling Modules for the Time-Digitizers, a CAMAC Crate Controller, and optionally, a Clock Prescaler Module. The Time-Digitizer Modules have 125 nsec time resolution and have eight input channels per single-width CAMAC module. The single channel analyzers in these modules have a software controllable lower discriminator level and each module has a common software-controllable upper discriminator level.

Each Data Collection System will also include a Central Data Corporation Z8001 single board microcomputer and bulk memory dedicated to data collection, transformation and storage. The microcomputer will accept the digitized data from the CAMAC System and will make the real-time transformations necessary to determine which memory location in the bulk memory should be incremented for a given detected neutron. A typical Data Collection System is also shown in Fig. 13.

Computers for the DAS have now been ordered and software development has begun on already available machines. Design and/or prototype testing is underway for the various hardware modules required. Construction has begun on a building to house the Host Computer System and some of the Minicomputer and Data Collection Systems. This building, scheduled to be completed this fall, will be located directly west of the main IPNS experiment hall (Building 375) and will also house data acquisition and control systems associated with the Radiation Effects Facility.

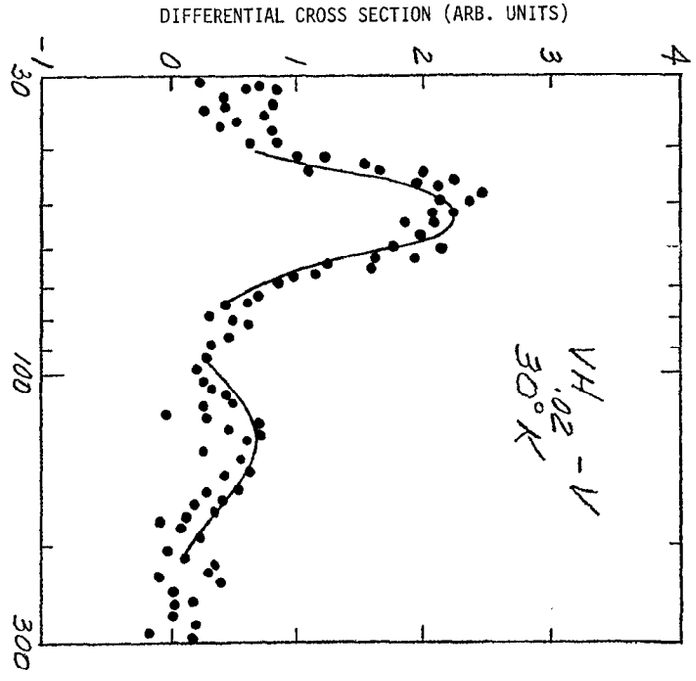

Fig. 1 Inelastic Neutron Scattering from $VH_{0.02}$, with V Scattering Subtracted

Time-of-flight spectra for UN under different conditons. Note the observation of the 1st, 2nd, and possibly even 3rd harmonic of the optic phonon mode with E_o = 307 meV. At low angle (ϕ = 7.5°) the phonon scattering is too weak to be seen.

FIG. 2

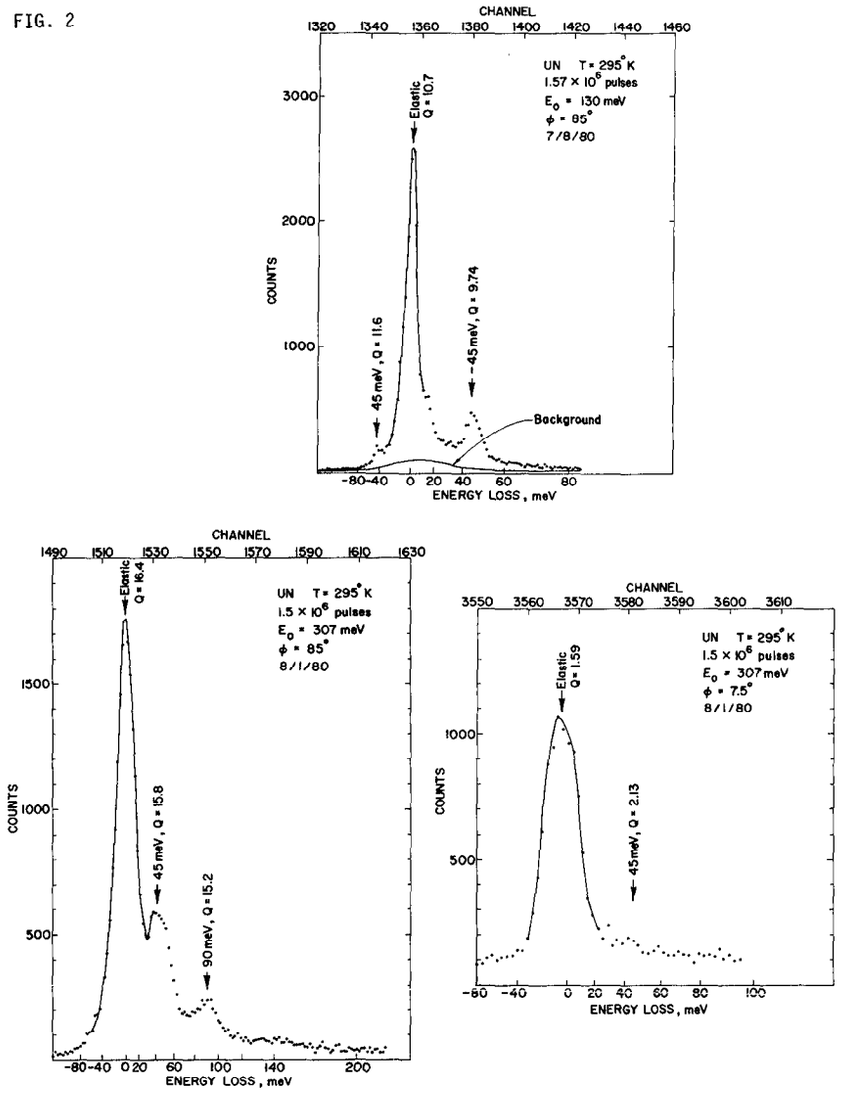

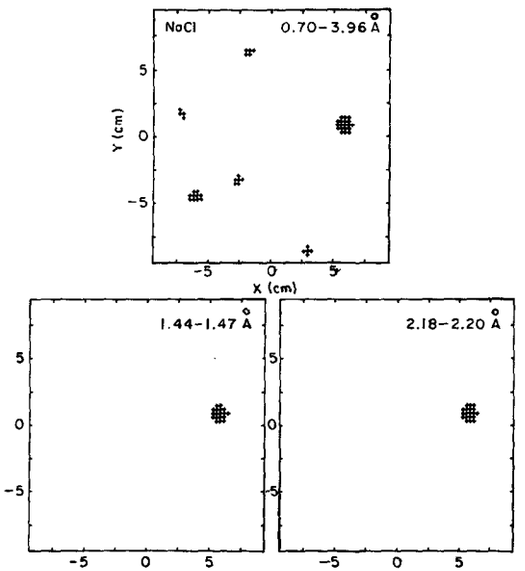

Fig. 3. Laue pattern from a NaCl crystal taken at ZING-P' with the NPSD. Upper section is summed over all energies (wavelengths) whereas lower sections show particular reflections.

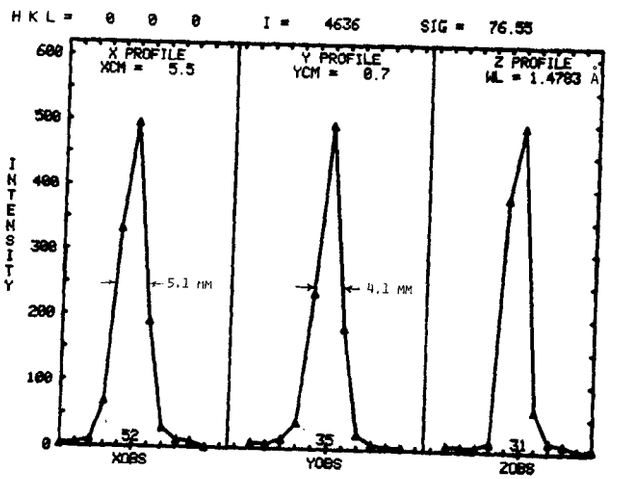

Fig. 4. Detail of Bragg peak in lower left of Fig. 3. Note the extremely good peak to background ratio in all three dimensions.

DATA COLLECTION FLOW DIAGRAM FOR IPNS SINGLE CRYSTAL DIFFRACTOMETER

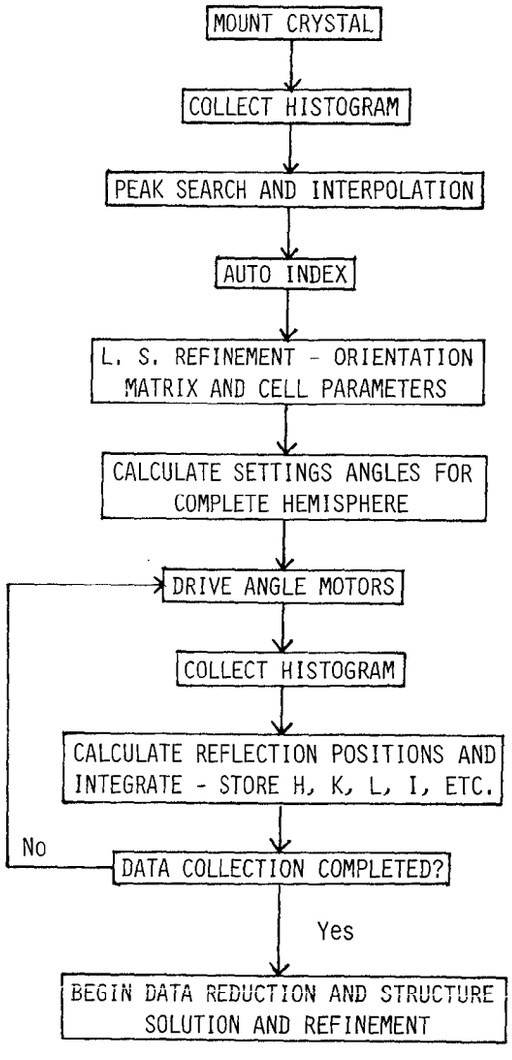

Fig. 5 Single Crystal Diffractometer Data Collection Flow Diagram

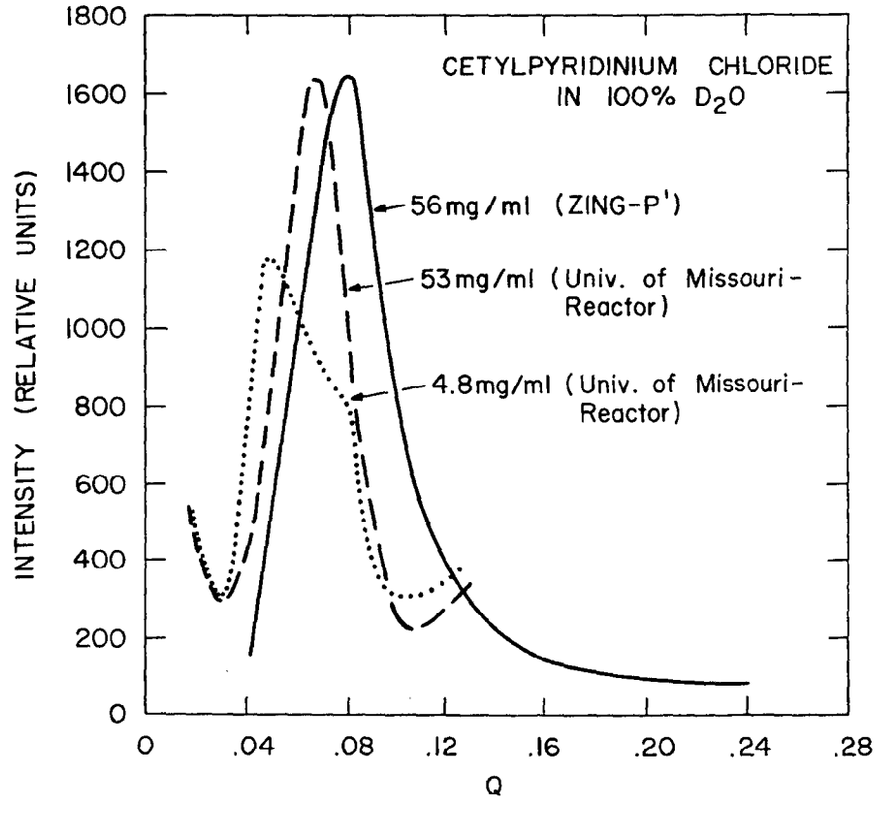

Fig. 6 Small-Angle Neutron Scattering from Cetylpyridinium Chloride

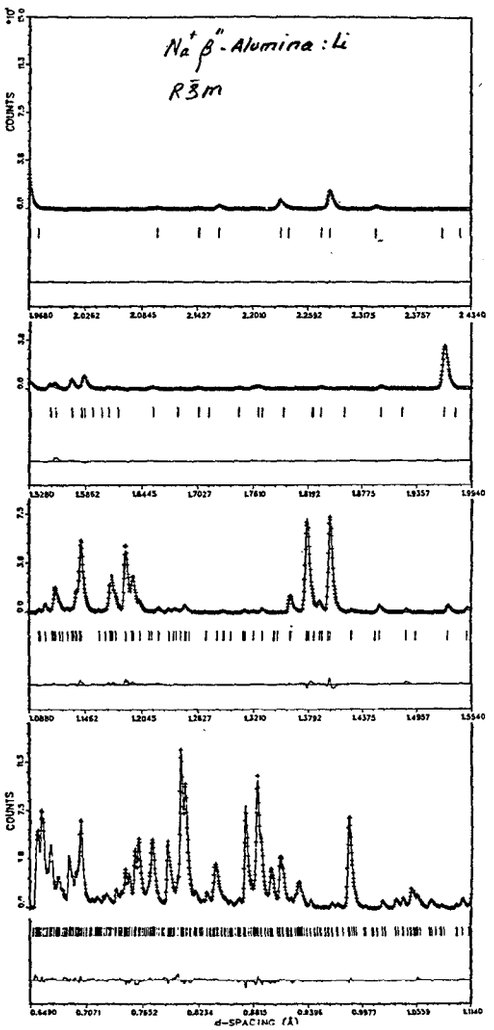

Fig. 7 Powder Diffraction Pattern from Li-Substituted Na-β"-alumina

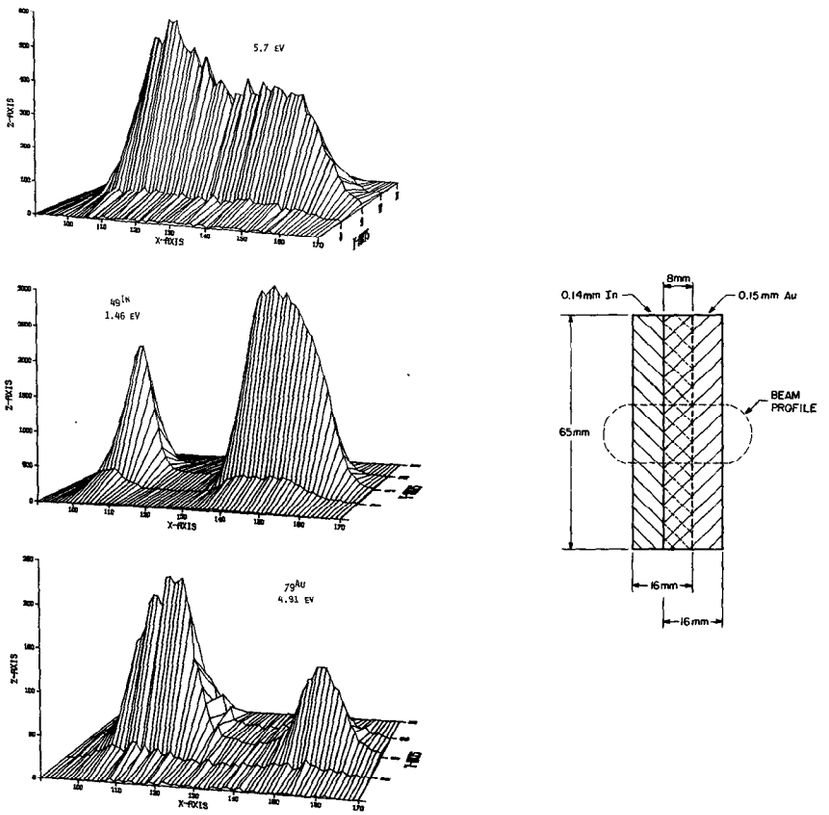

Fig. 8 The target is shown on the right. At the top is the spatial response at 5.7 eV, at which energy the target is almost transparent (see Fig. 9(a)). The center and lower sections are the spatial responses at the In and Au resonances, respectively, and clearly show the position of the foils.

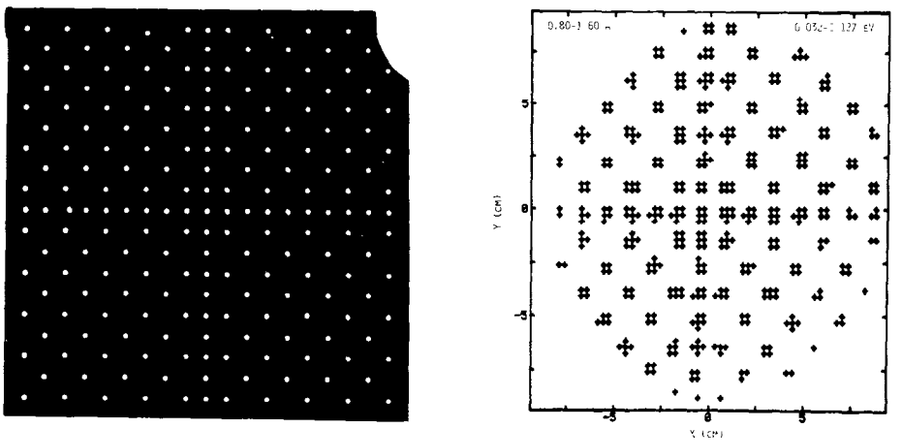

Fig. 10 Photograph (left) and output of NPSD on display screen (right) of cadmium mask. For the neutron pattern the mask was illuminated by scattering from a vanadium rod at ZING-P'.

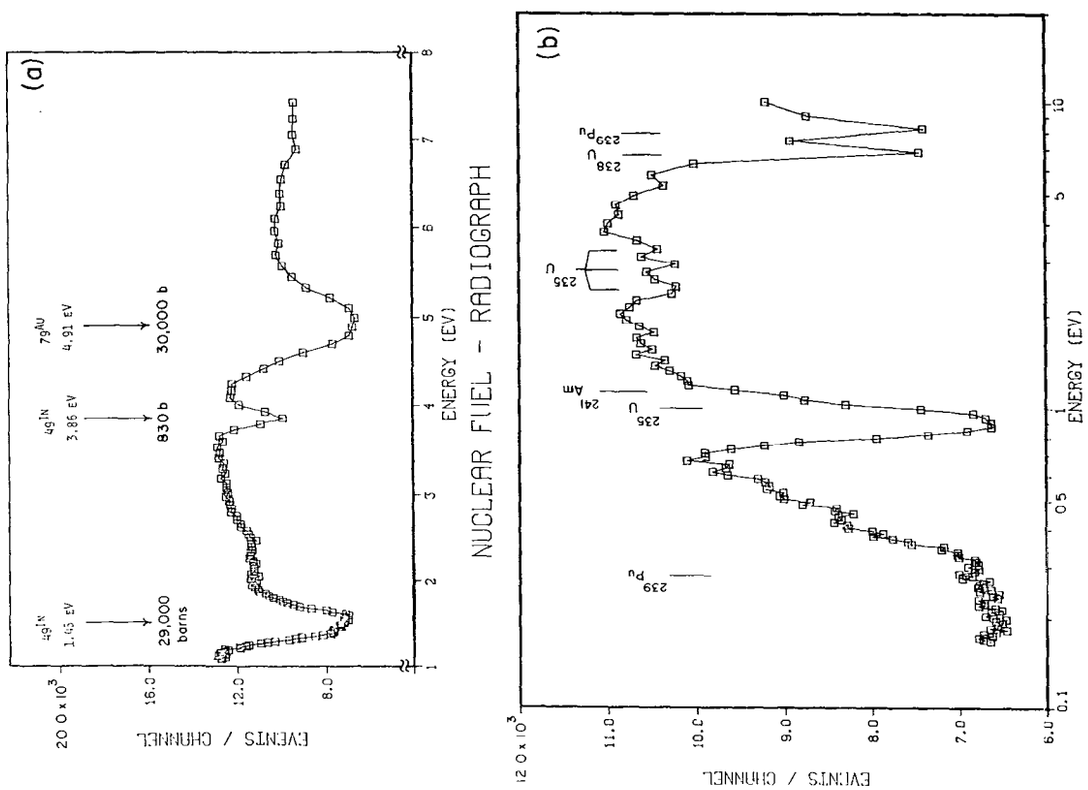

Fig. 9 Transmission Profile for (a) the Au-In Foil Target (see Fig. 8) and (b) the Nuclear Fuel Pellet

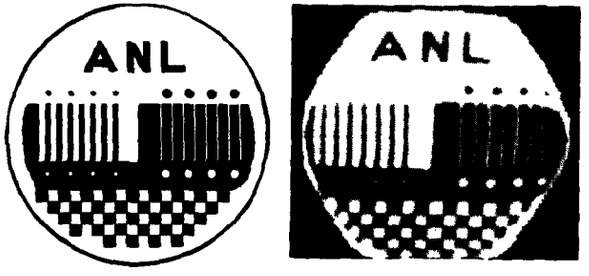

Fig. 11 Photograph (left) and output of NPSD on the display screen (right) of a BC_4 test pattern. See text for details of test pattern.

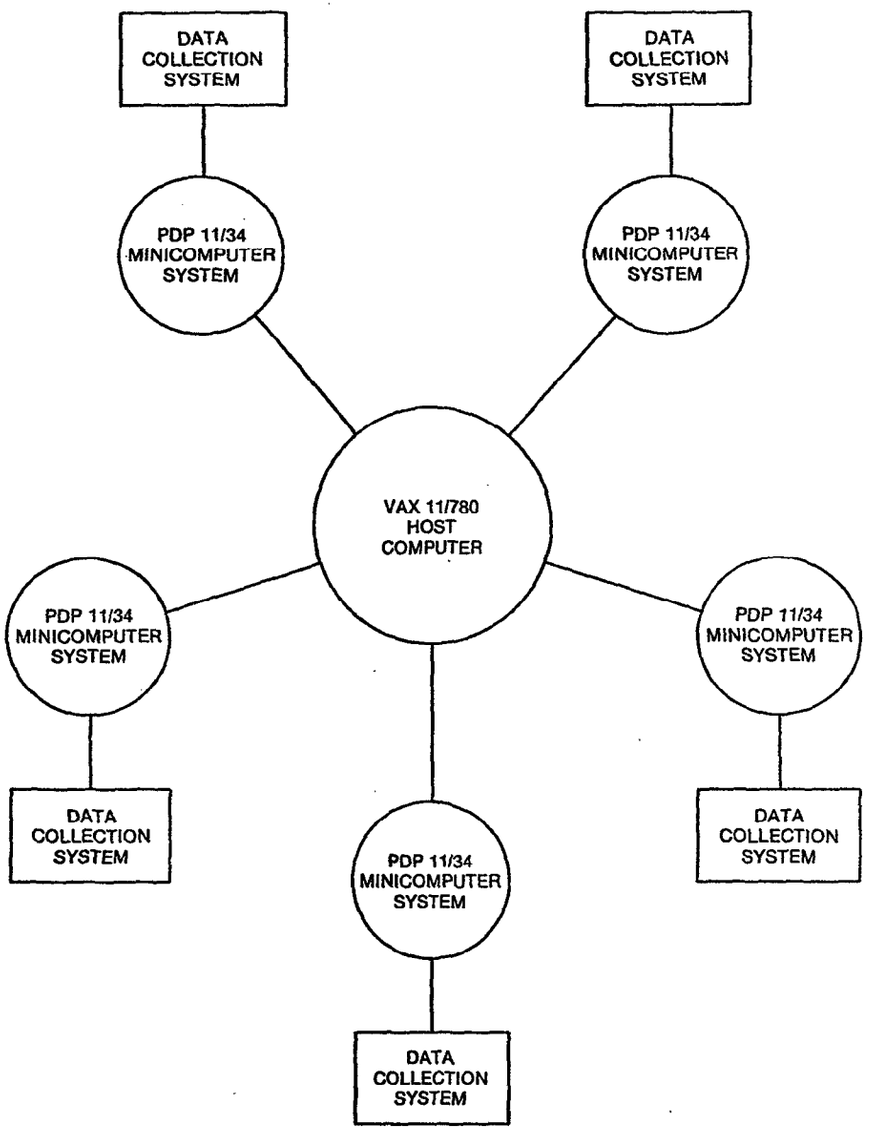

Fig. 12 The "star" configuration for the IPNS-I Data Acquisition System

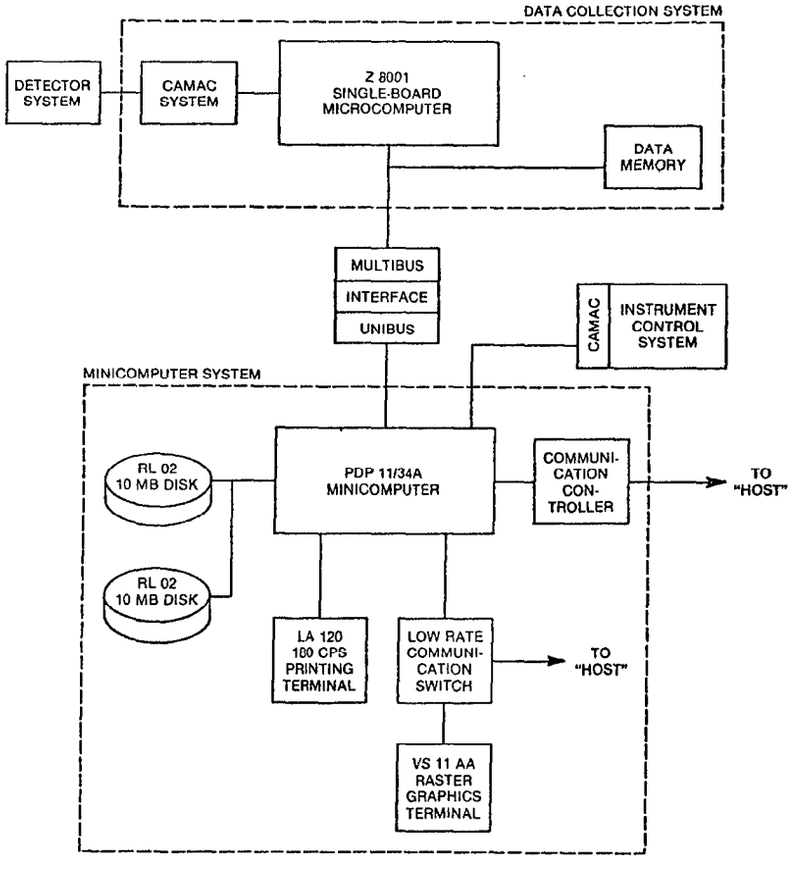

Fig. 13 Typical Minicomputer and Data-collection System for IPNS-I